Climate conformed to local supernova rates on geological timescales

Henrik Svensmark

National Space Institute, Technical University of Denmark

Juliane Marie Vej 30, 2100 Copenhagen Ø, Denmark

(Dated: February 20, 2009)

Abstract

Whether cosmic factors or atmospheric carbon dioxide, CO_2, were the main drivers of climate change during the Phanerozoic Eon has been a contentious issue for some years. Here the arguments are revisited, using on the one hand the supernova rates calculated from observations of open star clusters in the solar neighborhood, and on the other hand, paleosol data on CO_2. The supernova rates compare well with the paleoclimatology of the past 400 million years. The Earth was icy when supernovae were frequent and warm when the rate was low. Similarly, CO_2 levels were low when supernova rates were high, and vice versa, which explains why the prime driver appeared to be debatable.

PACS numbers: Valid PACS appear here

Shaviv[1–3] linked the icy episodes on the Earth during the 542 million years (Ma) of the Phanerozoic to the solar system's encounters with spiral arms of the Milky Way Galaxy during its orbit around the galactic center. He attributed the climatic effect to enhanced ionization of the air by galactic cosmic rays (GCR), in accordance with empirical evidence that these increase the low cloud cover[4–7]. So did Fuente Marcos and Fuente Marcos[8] in a study that used local star formation rates (SFR) as a proxy for GCR intensities. Since then, in a debate about whether GCR or atmospheric levels of carbon dioxide (CO_2) were more important in governing the climate on geological timescales[3, 9], there have been uncertainties on both sides. Estimates of past concentrations of CO_2 in the widely cited GEOCARB model[10] depend on quite complicated geochemical and tectonic modeling involving many parameters. On the astronomical side, the Galaxy's spiral pattern, its rotation speed and its density variations are all uncertain.

To sidestep such difficulties, in the hope of resolving an issue central to understanding Earth history during the main eon of plant and animal evolution, the aim here is to use the least 'model' dependent approach about the course of events in the remote past. In the case of CO_2, that means preferring the paleosol data, which usefully span about 400 Ma[9]. As for the GCR, open star clusters in the solar neighborhood are fossils of astrophysical activity over a similar timescale. A large fraction of star formation in the Galaxy is accounted for by cluster formation[11], and the ages of clusters are also a guide to the changing birth rate of massive stars that ended their lives as supernovae. As the shock fronts of massive-star supernovae are the main accelerators supplying GCR, the SN rate (supernovae per unit time) is here adopted as the proxy for GCR production. To achieve temporal resolution $\approx$8 Ma for comparisons with paleoclimatological data, the lifetimes of massive stars (up to 40 Ma) are taken into account.

The WEBDA database[12] contains about 1300 open star clusters with ages between 10^6 - 10^{10} y and at distances between 0.04 -13 kiloparsec (kpc). The present study uses 283 clusters that lie within 1 kpc of the solar system, have a distance less than 300 pc of the galactic plane, and the results will be restricted to the last 500 Ma. This sample is sufficiently large and statistically almost complete[13, 14]. A larger spatial sample would suffer from more and more undetected clusters at larger distances. The spatial scale of 1 kpc and temporal time steps of 8 Ma ensure that the GCR flux has had time to equilibrate with the newly appearing sources in the region. The resulting SN rate should therefore indicate

the changes in GCR flux experienced by the Earth's environment due to visits to high-SFR regions of the Galaxy (presumably in spiral arms) and low-SFR regions (presumably between spiral arms).

Open clusters are gravitationally bound sibling stars made in a single molecular cloud, but they gradually decay by the loss of stars, due to internal close encounters or to external encounters with massive clouds and other clusters. The resulting loss of old clusters can be seen in Fig. 1a, which shows the number of observed clusters as a function of age. The blue curve represents the fall-off with increasing age as a simple power law for the decay[15, 16], i.e. $dN/dt = at^{-\alpha}$ as illustrated by the blue line ($\propto t^{-\alpha+1}$) in Figure 1a. The fit to the observations gives α=1.50$\pm$0.07. This functional form of the decay can be used to normalize the cluster distribution, in order to estimate the cluster formation $C_F(t)$ as a function of time

$$C_F(t) = c_0 \frac{N(t)}{t^{-\alpha+1}}, \tag{1}$$

where c_0 is a constant. Fig. 1b shows the normalized cluster formation rate over the past 500 Ma, with the formation rate fluctuating widely around a long-term mean.

The final step is to deduce the number of supernovae SN in each 8 Ma bin. As open clusters are held together by their gravity, only massive groupings containing massive stars survive for long periods. The relative numbers of stars of various masses in a cluster is to a good approximation given by Salpeter's initial mass function (IMF) power law[17]. In consequence the number of stars going supernova will be, on average, proportional to the number of clusters in a bin, but the occurrences of the supernovae will spread into later bins. The evolution of stars in a cluster to their detonations as supernovae is simulated numerically by the Space Telescope Science Institute's Starburst99 program[18]. As seen in Fig. 2, if a stellar mass of 10^6 solar masses comes into being in an instantaneous starburst, supernovae first occur after $\approx$ 3 Ma and they continue for $\approx$ 40 Ma, until the last of the massive stars abruptly disappear. This form of the SN response function can be used to obtain the temporal variation in the SN rate caused by changes in the number of new clusters as

$$SN_{rate}(t) = c_{sn} \int_{-\infty}^{t} C_F(t') R_{SN}(t - t')\, dt', \tag{2}$$

where c_{sn} is a constant, $C_F(t)$ is the cluster formation history given by Eqn.(1) and shown in Fig. 1b, and finally R_{SN} is the SN response function to a starburst and shown in Fig. 1.

The numerical integration is displayed in Fig. 1c which shows the SN rates as a function of time. The SN rate is normalized to the present rate of SN in the solar neighborhood by taking the average of the two 24-16 and 16-8 Ma bins, ignoring the 8-0 Ma bin which is is misleadingly low because many new clusters are still hidden in dust. The present SN rate in the solar neighborhood is of the order 20 SN Ma^{-1} kpc^{-2}[19], which gives ≈500 SN for a typical 8 Ma bin and area of π kpc^2 (solar neighborhood).

As for the error bars in Fig, 1, the typical error in the age of a cluster is of the order 10-20%[8]. To estimate the resulting uncertainty by a bootstrap Monte Carlo method , 37% of the cluster ages, chosen at random in a sample, are replaced by a new age which is drawn from a random normal distribution with a 20% variance in the age and centered around the measured age. This process is repeated for 10^3 samples. The resulting variance in the number of clusters for each age bin is estimated and plotted as the error bars in Fig. 1a. Similarly the error bars in Fig. 1b and 1c are calculated by generating pseudo cluster distributions and calculating the resulting pseudo C_F and SN rates. Here the error bars increase with age due to the smaller relative number of observations of older clusters. A bootstrap Monte Carlo simulation adding Possion noise on the number of clusters increases the standard variation by $\approx 15\%$ in Fig. 1c.

An important assumption is that the majority of clusters have remained within 1 kpc of the solar system over the 500 Ma time span. Orbital diffusion of open clusters is not well understood but is expected to less than the diffusion of disk stars[8]. As the velocity dispersion of a disk star is expected to increase by 4% over the 500 Ma[20], movement of clusters in or out of the solar neighborhood is unlikely to be a severe problem, although it will tend to increase with the age of the clusters.

Although no assumptions were made about the Galaxy's spiral arms, in deriving the SN rate, the four maxima in Fig. 1c can, by the way, be interpreted as the solar system's encounters with four spiral arms, and used to extract information about the spiral structure at the solar circle. The black curve fitted to the maxima consists of four Gaussian functions. The functional form and parameters, shown in Table 1, suggest that maxima in SN occurred at intervals $\Delta t = (139.9, 149.5, 130.4)$ Ma intervals, averaging to $< \Delta t >= 140.1 \pm 6.4$ Ma. With the spiral pattern rotating at a smaller angular frequency Ω_P, the solar system moves in and out of the spiral arms with the relative angular frequency $\Delta\Omega = \Omega_0 - \Omega_P$ where $\Omega_0 = 25.9 \pm 4$ is the solar system rotation frequency, giving the pattern speed as

$\Omega_P = \Omega_0 - \pi/(2 < \Delta t >) = 14.7 \pm 4.0$ km s^{-1} kpc^{-1}. Although there has been a large range of estimates of the pattern speed, the value found here is in agreement with estimates derived in other ways, and is consistent with four spiral arm encounters of the solar system over the last 500 Ma[2, 20, 21]. The alternation between narrow and broad spiral arms seen in Fig. 2c may help to reconcile the four-arm and two-arm galactic maps currently on offer.

The delay between formation and detonation of massive stars has the effect, in Fig. 1c, of partly smoothing the very large variations from bin to bin seen in the cluster formation rate (Fig. 1b). Nevertheless, taking the SN rate in the solar neighborhood as a proxy for GCR at the Earth, the plot implies that persistent ionization in the lower atmosphere due to GCR went up and down twice by a factor of ≈2 over 500 Ma. As shown in Fig. 3, cool conditions prevailed when SN rates were high, and warmer intervals when they were lower.

The paleoclimatic data in the upper panels in Fig. 3 come from two well-respected sources, namely Crowley[22] for the latitudes attained by continental ice, and Frakes et al.[23] for the divisions of the Paleozoic timescale into warm and cool modes. Their dates are here adjusted to the current geological timescale[24]. More precise timings of some climatic extremes, available recently, fit the SN curve surprisingly well, including a glaciation peak 294 to 289 Ma ago [25] and a rapid rise in CO_2 associated with global warming of 6.5 °C that occurred about 183 Ma ago[26], suggesting that that the broad match between SN rates and climate is not coincidental. An impression the overall temperature range comes from In situ measurements of δ^{18}O using ion microprobes in Ordovician conodont fossils, by Trotter et al.[27], who estimate a sea surface cooling of ≈16 °C between 489 and 443 Ma ago. In this ancient case the reported cooling begins about 30 Ma earlier, and peaks about 15 Ma earlier, than the SN curve would suggest, a discrepancy which is unsurprising in view of the 10-20% error in cluster dates, and relatively poor statistics on the few surviving clusters at this age.

Fig. 3 also compares SN rates and atmospheric CO_2 concentrations, with the latter plotted upside down because high SN rates and low CO_2 go together. The proxy used here for CO_2 is δ^{13}C in paleosols, offers the longest time-span among the various proxies, although it is less accurate than other proxies at low CO_2[28, 29]. The similarity between the astronomical and CO_2 variations is striking (correlation coefficient, $r = -0.76$). The difficulty in telling whether variations in GCR or CO_2 offered the better match to paleoclimates[3, 9] may now be explained because a causal connection seemed to have them made almost equally close.

CO_2 was low during cool modes, just as expected by the greenhouse hypothesis, but these were also times of high SN rates. No event on the Earth could conceivably influence star formation hundreds of parsecs away, so cause and effect can have gone only in one direction. The most straightforward inference from Fig. 3 is that star-driven climate changes drove, in turn, the processes that are responsible for variations in atmospheric CO_2 concentrations.

More generally, the match of climate to SN rates, seen in Fig. 3, leaves room only for relatively small or brief influences of all the tectonic, volcanic, and other processes discussed by geologists. If the dominant role of the Galaxy in the terrestrial environment is further validated by ongoing studies, cosmic and terrestrial, it promises to simplify Phanerozoic climatology.

---

[1] N. J. Shaviv, Physical Review Letters **89**, 051102 (2002), arXiv:astro-ph/0207637.

[2] N. J. Shaviv, New Astronomy **8**, 39 (2003), arXiv:astro-ph/0209252.

[3] N. Shaviv and J. Veizer, GSA Today **14**, 18 (2004).

[4] H. Svensmark and E. Friis-Christensen, J. Atmos. & Solar Terr. Phys. **59**, 1225 (1997).

[5] H. Svensmark, Phys. Rev. Lett. **81**, 5027 (1998).

[6] N. D. Marsh and H. Svensmark, Phys. Rev. Lett. **85**, 5004 (2000).

[7] H. Svensmark, Astronomy and Geophysics **48**, 010000 (2007).

[8] R. de La Fuente Marcos and C. de La Fuente Marcos, New Astronomy **10**, 53 (2004), arXiv:astro-ph/0405451.

[9] D. L. Royer, R. A. Berner, I. P. Montaez, N. J. Tabor, and D. J. Beerling, GSA Today **14**, 4 (2004).

[10] R. A. Berner and Z. Kothavala, Am J Sci **301**, 182 (2001), http://www.ajsonline.org/cgi/reprint/301/2/182.pdf, URL `http://www.ajsonline.org/cgi/content/abstract/301/2/182`.

[11] C. J. Lada and E. A. Lada, Annurev. Astro **41**, 57 (2003), arXiv:astro-ph/0301540.

[12] Open Cluster Database, http://www.univie.ac.at/webda/ (2009).

[13] R. Wielen, A&A **13**, 309 (1971).

[14] A. E. Piskunov, N. V. Kharchenko, S. Röser, E. Schilbach, and R.-D. Scholz, A&A **445**, 545 (2006), URL `http://dx.doi.org/doi/10.1051/0004-6361:20053764`.

[15] R. Chandar, S. M. Fall, and B. C. Whitmore, ApJ **650**, L111 (2006), arXiv:astro-ph/0609360.

[16] R. de la Fuente Marcos and C. de la Fuente Marcos, ApJ **672**, 342 (2008).

[17] E. E. Salpeter, ApJ **121**, 161 (1955).

[18] C. Leitherer, D. Schaerer, J. Goldader, R. Delgado, C. Robert, D. Kune, D. deMello, D. Devost, and T. Heckman, The Astrophysical Journal Supplement Series **123**, 3 (1999), http://www.journals.uchicago.edu/doi/pdf/10.1086/313233, URL `http://www.journals.uchicago.edu/doi/abs/10.1086/313233`.

[19] I. A. Grenier, A&A **364**, L93 (2000), arXiv:astro-ph/0011298.

[20] D. R. Gies and J. W. Helsel, ApJ **626**, 844 (2005), arXiv:astro-ph/0503306.

[21] H. Svensmark, Astronomische Nachrichten **327**, 866 (2006).

[22] T. Crowley, *Significance of Tectonic Boundary Conditions for Paleoclimate Simulations* (Tectonic Boundary Conditions for Climate Reconstructions, Edited by T. Crowley and K. Burke, pp. 3. Oxford University Press US, 1998, 1998).

[23] L. A. Frakes, J. E. Francis, and J. I. Syktus, *Climate Modes of the Phanerozoic* (Cambridge Monographs in Physics, 1992).

[24] F. M. Gradstein, J. G. Ogg, and A. G. Smith, *A Geologic Time Scale 2004* (A Geologic Time Scale 2004, Edited by Felix M. Gradstein and James G. Ogg and Alan G. Smith, pp. 610. ISBN 0521781426. Cambridge, UK: Cambridge University Press, April 2005., 2005).

[25] C. Fielding, T. Frank, and J. Isbell, GSA Special Paper 441: Resolving the Late Paleozoic Ice Age in Time and Space **441**, 343 (2008).

[26] J. C. McElwain, J. Wade-Murphy, and S. P. Hesselbo, Nature **435**, 479 (2005).

[27] J. A. Trotter, I. S. Williams, C. R. Barnes, C. Lécuyer, and R. S. Nicoll, Science **321**, 550 (2008).

[28] D. L. Royer, R. A. Berner, and D. J. Beerling, Earth Science Reviews **54**, 349 (2001).

[29] D. L. Royer, Geochimica et Cosmochimica Acta **70**, 5665 (2006).

Acknowledgments

The author thanks Nigel Calder for discussions regarding this work. This research has made use of the WEBDA database (http://www.univie.ac.at/webda/) , operated at the Institute for Astronomy of the University of Vienna

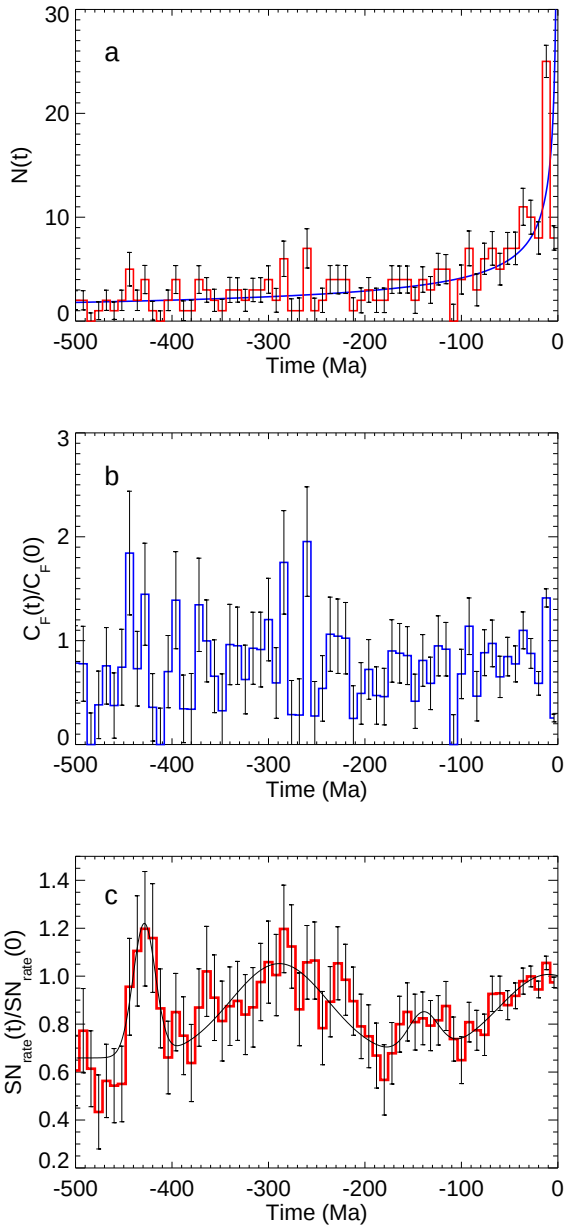

FIG. 1: To derive variations in the local supernova rate over 500 million years (Ma), the numbers of open star clusters within 1 kpc of the solar system, that originated in each 8 Ma bin, are plotted in Fig. 2 a. The low count of clusters less than 8 Ma old, compared with that in the 8-16 Ma bin, is probably due to their concealment by natal dust clouds that have not yet dissipated. The more general fall, going back 500 Ma, is the result of clusters decaying by the escape of stars, and the blue curve is a power law that describes this decay (see text). When it is taken into account, the formation rates of clusters over 500 Ma are derived, as in Fig. 2b. There is a large variation between the lowest and highest rates. The C_F rate is normalized by taking the average of the two 24-16 and 16-8 Ma bins. In Fig. 2c, application of the supernova response function illustrated in Fig. 3 gives the supernova rate per 8 Ma. The calculation of error bars is explained in the text.

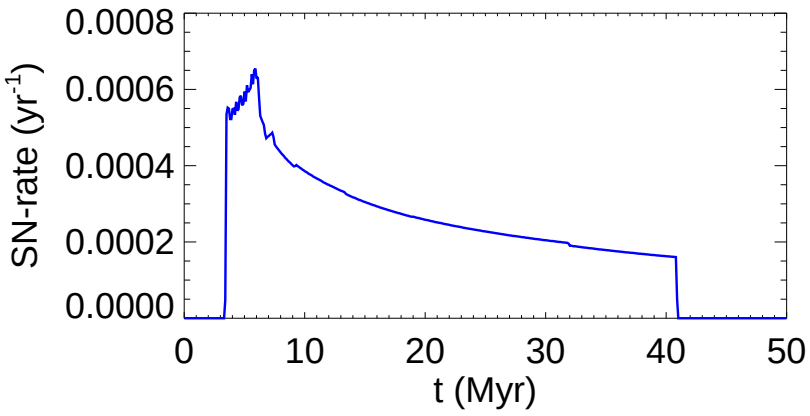

FIG. 2: Response function of supernovae resulting from an initial starburst of stellar mass 10^6 $M_\odot$ at t=0, as calculated by Starburst99[18]. (Parameters of the simulation. Two IMF intervals, with exponents 1.3, 2.3 at mass boundaries 0.1, 0.5, 100 $M_\odot$, supernova cut-off mass 8 $M_\odot$, black hole cut-off mass 100 $M_\odot$, metallicity 0.020 and PADOVA track with AGB stars.)

Arm	Perseus	Norma	Scutum-Crux	Sgr-Car
t_0	-428.8	-288.9	-139.4	-9.0
σ	11.5	50.6	15.7	51.7
A	0.55	0.39	0.17	0.34

TABLE I: Model parameters of the function ($M = A_0 + \sum_{i=1}^{4} A_i \exp[-(t - t_0^i)^2/2\sigma_i^2]$) used in Fig. 2c (black curve). (t_0 and σ in units of Ma and $A_0 = 0.65$)

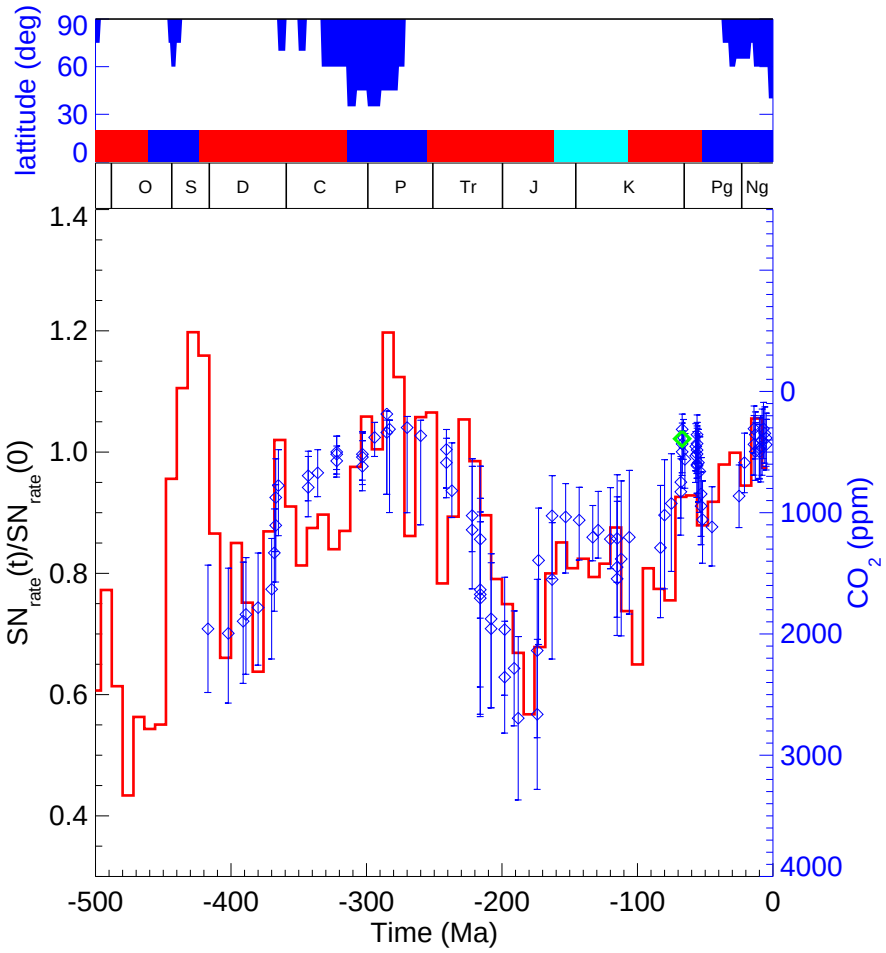

FIG. 3: Used here as a proxy for galactic cosmic rays (GCR) reaching the Earth, the local supernova rate (red curve) from Fig. 1c is compared with paleoclimatic data (upper panel) and with concentrations of CO_2 in the air (blue diamonds, scale inverted). Abbreviations for geological periods are: Cm, Cambrian; O, Ordovician; S, Silurian; D, Devonian; C, Carboniferous; P, Permian; Tr, Triassic; J, Jurassic; K, Cretaceous; Pg, Paleogene; Ng, Neogene. Following Crowley[22], the vertical blue bars at the top depict the latitudinal reach of continental glaciation (the lower, the colder) whilst the alternation of warm (red) and cold (blue) modes derives from Frakes et al.[23]. The light blue in Cretaceous indicate a milder cold period. A general match of glacial conditions to high GCR, and warm conditions to low GCR, is readily apparent, and two particular "hits" with climatic conforming to high and low SN rates are noted in the text. The CO_2 plots are from $\delta^{13}C$ in paleosols, and follow Royer[9] in using a five-point running average of the CO_2 values. For the sake of visual clarity, 42 high resolution CO_2 measurements from the interval 70-64 Ma are averaged and plotted as one point (green).